East Eur. J. Phys. Vol.1 No.1 (2014) 4-20

PACS: 21.60.Jz, 21.65.Ef, 21.10.Gv, 21.30.Fe, 27.40.+z, 27.50.+e

STRUCTURE PROPERTIES OF NEUTRON-RICH EXOTIC NUCLEI

A.N. Antonov*, M.K. Gaidarov*, P. Sarriguren†, E. Moya de Guerra**
**Institute for Nuclear Research and Nuclear Energy, Bulgarian Academy of Sciences*
Sofia 1784, Bulgaria
†Instituto de Estructura de la Materia, IEM-CSIC
Serrano123, E-28006 Madrid, Spain
***Departamento de Fisica Atomica, Moleculary Nuclear, Facultad de Ciencias Fisicas, Universidad Complutense de Madrid*
E-28040 Madrid, Spaine
e- mail: aantonov@inrne.bas.bg
Received February 11, 2014

Theoretical study of important bulk properties of nuclei far from stability such us the nuclear skin and its correlation with the density dependence of the symmetry energy in uniform matter is reviewed. The formation of neutron skin and its evolution with an increase of the neutron number is investigated on the basis of a self-consistent deformed mean-field Hartree-Fock method using density-dependent Skyrme force sand pairing correlations in BCS approach. We study isotopic chains of Ni, Kr, and Sn nuclei and consider all the experimentally observed isotopes from neutron-deficien to neutron-rich ones. Various definition of the neutron skin thickness based on the differences between neutron and proton radii as well as on comparison of the tail soft he neutron and proton density distributions have been tested. The effects of deformation on the neutron skins in even-even deformed nuclei are discussed on the example of Kr isotopes. The symmetry energy, the neutron pressure and the asymmetric compressibility of spherical Ni, Sn, and Pb and deformed Kr and Sm neutron-rich even-even nuclei are calculated within the coherent density fluctuation model using the symmetry energy as a function of density within the Brueckner energy-density functional. The correlation between the thickness of the neutron skin and the characteristics related with the density dependence of the nuclear symmetry energy is investigated for isotopic chains of these nuclei. The mass dependence of the nuclear symmetry energy and the neutron skin thickness are also studied together with the role of the neutron-proton asymmetry. The studied correlations reveal a smoother behavior in the case of spherical nuclei than for deformed ones. We also note that the neutron skin thickness obtained for ^{208}Pb with SLy4 force is found to be in a good agreement with the recent data. In addition, we analyse the existence of peculiarities of the studied quantities in Ni and Sn isotopic chains that are not present in the Pb chain.
KEYWORDS: exotic nuclei, neutron skin thickness, symmetry energy, deformed Hartree-Fock+BCS method, energy-density functional

INTRODUCTION

The detailed study of the properties of unstable nuclei has been at the fore front of nuclear physics research for the past few years. The ultimate goal of such studies is to develop models and interaction potentials by uncovering novel manifestations of nuclear structure when moving away from the valley of stability, among which nuclear haloes and skins, new regions of nuclear deformation, the disappearance of shell closures or the appearance of new magic numbers may be cited. The most straightforward way to assess the presence of such phenomena is to follow nuclear properties along extended isotopic chains analyzing contrasted behaviors between stable and unstable species.

The determination of charge radii and extraction of nuclear matter radii are crucial for studying the evolution of neutron and proton skins along isotopic chains. To get information on the neutron skin thickness one needs data obtained with probes having different sensitivities to the proton and neutron distributions. The methods for extracting the neutron skin thickness mostly include experiments on hadron scattering [1,2], antiprotonic atoms [3], parity violating electron scattering [4,5,6], a swell as giant dipole resonance method [7] and spin-dipole resonance method [8,9].

On the theoretical side, calculations of nuclear charge and matter radii of exotic nuclei are usually performed in the framework of mean-field approaches, namely the Hartree-Fock (HF) method or the Hartree-Fock-Bogoliubov (HFB) method including pairing correlations (e.g., Ref. [10]). Recently, the self-consistent relativistic mean-fiel (RMF) model has been widely applied to studies of both stable and unstable nuclei (e.g., Ref. [11]). Many calculations show that the RMF model can reproduce with a good precision a number of ground-state nuclear properties including the charge radii [12]. The charge rms radii were successfully described in Ref.[10], where the generator coordinate method (GCM) on top of Gogny HFB calculations was explored.

Theoretical identification of the skin structure in neutron-rich weakly bound nuclei, however, is still a matter of discussion. In Ref. [13] a definition of the neutron skin and its appearance were presented in terms of spherical HF calculations. The proposed criteria which deal with proton and neutron densities allowed one to predict neutron skins in nuclei far from the β stability line. The Helm model [14, 15] has been applied in Ref. [16] to analyze neutron and proton skins, as well as halos, of even-even Ni, Sn, and Pb isotopes in terms of form factors.

Recently, the interest in the symmetry energy has been stirred up by novel astrophysical observations and by the availability of exotic beams in accelerators that provide additional information to the standard nuclear asymmetry studies based on stable nuclei. Particularly important in the different areas, and similarly uncertain, is the density dependence of the symmetry energy in uniform matter. The neutron skin thickness, generally defined as the difference between neutron and proton rms radii in the atomic nucleus, is closely correlated with this dependence. Moreover, it has been shown that the neutron skin thickness in heavy nuclei, like ^{208}Pb, calculated in mean-field models with either nonrelativistic or relativistic effective nuclear interactions, displays a linear correlation with the slope of the neutron equation of state (EOS) obtained with the same interactions at a neutron density $\rho \approx 0.10$ fm^{-3} [17, 18].

The ground states of atomic nuclei are characterized by different equilibrium configurations related to corresponding geometrical shapes. The study of the latter, as well as the transition regions between them, has been a subject of a large number of theoretical and experimental studies (for a review, see, for example, Ref. [19] and references therein). The position of the neutron drip line is closely related to the neutron excess and the deformation in nuclei. In fact, the latter increases the surface area, thus leading to a larger surface symmetry energy in a neutron-rich nucleus with a deformed shape. Conversely, the precise determination of the surface symmetry energy is important to describe the deformability of neutron-rich systems and also to validate theoretical extrapolations. Therefore, it is worth to explore how the nuclear symmetry energy changes in the presence of deformation and correlates with the neutron skin thickness within a given isotopic chain.

Nowadays, the experimental information about the symmetry energy is fairly limited. The need to have information about this quantity in finite nuclei, even theoretically obtained, is a major issue because it allows one to constrain the bulk and surface properties of the nuclear energy-density functionals quite effectively. The symmetry energy of finite nuclei at saturation density is often extracted by fitting ground state masses with various versions of the liquid-drop mass formula within liquid-drop models [20, 21, 22]. It has been also studied in the random phase approximation based on the Hartree-Fock (HF) approach [23] or effective relativistic Lagrangians with density-dependent meson-nucleon vertex functions [24], energy density functionals of Skyrme force [25, 26] as well as relativistic nucleon-nucleon interaction [27, 28].

In the present review (as well as in Refs. [29, 30, 31]), the properties of a wide range of medium and heavy exotic nuclei are described using the self-consistent deformed mean-field Hartree-Fock method with density dependent Skyrme interactions [32, 33] and pairing correlations. Pairing between like nucleons has been included by solving the BCS equations at each iteration either with a fixed pairing gap parameter (determined from the odd-even experimental mass differences) or with a fixed pairing strength parameter. In our calculations the following Skyrme force parametrizations are used: SLy4 [34], SGII [35], Sk3 [36], and LNS [37]. These are among the most extensively used Skyrme forces and are considered as standard references.

The main aim of this study is twofold. First, to clarify theoretically the emergence of the neutron and proton skins in neutron-rich and neutron-deficient isotopes, respectively, by testing different definitions for the skin thickness in the framework of the deformed Skyrme HF+BCS model. We choose isotopes of some medium and heavy nuclei such as Ni (A=48–78), Kr (A=70–100), and Sn (A=100–136) because many of these sets, which lie in the nuclear chart between the proton and neutron drip lines can be formed as radioactive ions to perform scattering experiments. Alternatively to one of the criteria for the neutron skin proposed in Ref. [13] we consider another one which treats proton and neutron densities in a similar way. The calculated charge rms radii are compared with the laser or muonic atoms spectroscopy measurements of isotope shifts performed on Sn [38, 39, 40, 41], Ni [42, 43], and Kr [44] isotopes. Our theoretically calculated neutron skin thicknesses are compared with the available experimental data extracted from methods mentioned above for even-even Sn isotopes with masses from 112 to 124. We also study whether the emergence of a skin is influenced by the nuclear shape, an issue that has not been sufficiently studied so far. The question of the skin formation in nuclei having a non-spherical shape is discussed in detail on the example of Kr isotopes, assuming axial symmetry.

Second, in addition to various linear relations between several quantities in bulk matter and for a given nucleus that have been observed and tested within different theoretical methods (e.g. nonrelativistic calculations with different Skyrme parameter sets and relativistic models), we establish a correlation between the skin thickness and some nuclear matter properties in finite nuclei, such as the symmetry energy s, the symmetry pressure p_0 (proportional to the slope of the bulk symmetry energy), and the asymmetric compressibility ΔK, clarifying to what extent this correlation is appropriate for a given isotopic chain. The symmetry energy is studied on the basis of the Brueckner energy-density functional for nuclear matter [45, 46] and using the coherent density fluctuation model (CDFM) (e.g., Refs. [47, 48, 49]). The CDFM has been successfully applied to different tasks: to calculate nuclear properties of the ground and first monopole states, in scaling analyses and others. In addition to some spherical medium and heavy Ni (A=74-84) and Sn (A=124-152) isotopes (considered also in Refs. [29, 50]), we present results for a chain of Pb (A=202-214) isotopes being inspired by the significant interest (in both experiment [51, 52, 53] and theory [54, 55, 56, 57]) to study, in particular, the neutron

distribution of ^{208}Pb and its rms radius. An investigation of the same possible relation is carried out for chains of deformed neutron-rich even-even Kr (A=82-96) (including, as well, the case of some extreme neutron-rich nuclei up to ^{120}Kr) and Sm (A=140-156) isotopes. At the end we give some numerical arguments in proof of the existence of some peculiarities in the properties of Ni and Sn isotopic chains that are not present in the Pb chain.

DEFORMED SKYRME HF+BCS FORMALISM

Assuming time reversal, the single-particle Hartree-Fock solutions for axially symmetric deformed nuclei are characterized by the eigenvalue Ω_i of the third component of the total angular momentum on the symmetry axis and by the parity π_i. The state i can be written as

$$\Phi_i\left(\vec{R},\sigma,q\right)=\chi_{q_i}(q)\left[\Phi_i^+(r,z)e^{i\Lambda^-\varphi}\chi_+(\sigma)+\Phi_i^-(r,z)e^{i\Lambda^+\varphi}\chi_-(\sigma)\right], \tag{1}$$

where $\chi_{q_i}(q)$, $\chi_\pm(\sigma)$ are isospin and spin functions, $\Lambda^\pm=\Omega_i\pm 1/2\geq 0$. r,z,φ are the cylindrical coordinates of $\vec{R}$.

The wave functions Φ_i are expanded into the eigenfunctions, ϕ_α, of an axially symmetric deformed harmonic-oscillator potential in cylindrical coordinates. We use 12 major shells in this expansion,

$$\Phi_i\left(\vec{R},\sigma,q\right)=\chi_{q_i}(q)\sum_\alpha C_\alpha^i\phi_\alpha\left(\vec{R},\sigma\right), \tag{2}$$

with $\alpha=\{n_r,n_z,\Lambda,\Sigma\}$ and

$$\phi_\alpha\left(\vec{R},\sigma\right)=\psi_{n_r}^\Lambda(r)\psi_{n_z}(z)\frac{e^{i\Lambda\varphi}}{\sqrt{2\pi}}\chi_\Sigma(\sigma), \tag{3}$$

in terms of Hermite and Laguerre polynomials

$$\psi_{n_z}(z)=\sqrt{\frac{1}{\sqrt{\pi}2^{n_z}n_z!}}\,\beta_z^{1/2}e^{-\xi^2/2}H_{n_z}(\xi), \tag{4}$$

$$\psi_{n_r}^\Lambda(r)=\sqrt{\frac{n_r}{(n_r+\Lambda)!}}\,\beta_\perp\sqrt{2}\,\eta^{\Lambda/2}e^{-\eta/2}L_{n_r}^\Lambda(\eta), \tag{5}$$

with

$$\begin{aligned}\beta_z=(m\omega_z/\hbar)^{1/2}\quad,\qquad \beta_\perp=(m\omega_\perp/\hbar)^{1/2},\\ \xi=z\beta_z\quad,\qquad \eta=r^2\beta_\perp^2.\end{aligned} \tag{6}$$

The spin-independent proton and neutron densities are given by

$$\rho(\vec{R})=\rho(r,z)=\sum_i 2v_i^2\rho_i(r,z), \tag{7}$$

in terms of the occupation probabilities v_i^2 resulting from the BCS equations and the single-particle densities ρ_i. The multipole decomposition of the density can be written as [32]

$$\rho(r,z)=\sum_\lambda\rho_\lambda(R)P_\lambda(\cos\theta)=\rho_0(R)+\rho_2(R)P_2(\cos\theta)+\ldots, \tag{8}$$

with multipole components λ

$$\rho_\lambda(R)=\frac{2\lambda+1}{2}\int_{-1}^{+1}P_\lambda(\cos\theta)\rho(R\cos\theta,R\sin\theta)d(\cos\theta), \tag{9}$$

and normalization given by

$$\int\rho(\vec{R})d\vec{R}=X;\qquad 4\pi\int R^2dR\rho_0(R)=X, \tag{10}$$

with $X=Z,N$ for protons and neutrons, respectively.

The mean square radii for protons and neutrons are defined as

$$<r_{\rm p,n}^2>=\frac{\int R^2\rho_{\rm p,n}(\vec{R})d\vec{R}}{\int\rho_{\rm p,n}(\vec{R})d\vec{R}}, \tag{11}$$

and correspondingly, the root-mean square (rms) radii for protons and neutrons are given by

$$r_{\rm p,n} = < r^2_{\rm p,n} >^{1/2} \ . \tag{12}$$

The mean square radius of the charge distribution in a nucleus can be expressed as

$$< r^2_{\rm ch} > = < r^2_{\rm p} > + < r^2_{\rm ch} >_{\rm p} + (N/Z) < r^2_{\rm ch} >_{\rm n} + r^2_{\rm CM} + r^2_{\rm SO} \, , \tag{13}$$

where $< r^2_{\rm p} >$ is the mean square radius of the point proton distribution in the nucleus (11), $< r^2_{\rm ch} >_{\rm p}$ and $< r^2_{\rm ch} >_{\rm n}$ are the mean square charge radii of the charge distributions in a proton and a neutron, respectively. $r^2_{\rm CM}$ is a small correction due to the center of mass motion, which is evaluated assuming harmonic-oscillator wave functions. The last term $r^2_{\rm SO}$ is a tiny spin-orbit contribution to the charge density. Correspondingly, we define the charge rms radius

$$r_{\rm c} = < r^2_{\rm ch} >^{1/2} \ . \tag{14}$$

NEUTRON SKINS IN EXOTIC NUCLEI

To study the neutron skin thickness we will use first the difference between the neutron and proton rms radii to characterize the different spatial extensions of neutron and proton densities. A more effective tool to analyze skins [16], however, is the Helm model [14, 15]. This is a model that allows one to extract in a simple way from the form factor the two main characteristics of the density, a diffraction radius and a surface thickness. In this model one describes the density by convoluting a hard sphere (hs) density having diffraction radius R_d with a gaussian of variance σ,

$$\rho_{\rm Helm}(r; R_d, \sigma) = \rho_{\rm hs}(r; R_d) * \rho_G(r; \sigma) \, , \tag{15}$$

where

$$\rho_{\rm hs}(r, R_d) = \frac{3X}{4\pi R_d^3} \Theta(R_d - r), \tag{16}$$

and

$$\rho_G(r; \sigma) = (2\pi\sigma^2)^{-3/2} e^{(-r^2/2\sigma^2)}. \tag{17}$$

The corresponding Helm form factor is

$$F_{\rm Helm}(q) = F_{\rm hs}(q; R_d) F_G(q; \sigma) = \frac{3}{qR_d} j_1(qR_d) e^{-\sigma^2 q^2/2} \, . \tag{18}$$

Now, the most prominent feature of the density distribution, namely its extension, can be related to the first zero in the form factor, this is the diffraction radius

$$R_d = 4.49341/q_1 \, , \tag{19}$$

where q_1 is the first zero of the form factor. The nuclear surface width σ can be related to the height of the second maximum of the form factor located at $q_{\rm max}$:

$$\sigma^2 = \frac{2}{q^2_{\rm max}} \ln \frac{3 j_1(q_{\rm max} R_d)}{R_d q_{\rm max} F(q_{\rm max})} \, . \tag{20}$$

Taking into account that the second moment of a convoluted distribution is given by the sum of the second moments of the two single distributions, one gets the Helm rms radius

$$R^{\rm Helm}_{\rm rms} = \sqrt{\frac{3}{5} \left(R_d^2 + 5\sigma^2 \right)} \, . \tag{21}$$

Taking out the factor $\sqrt{3/5}$, that relates the rms radii to the radii of the equivalent uniform hard spheres, we define

$$R_{\rm hs} = \sqrt{5/3} < r^2 >^{1/2} \tag{22}$$

and

$$R_{\rm Helm} = \sqrt{5/3} R^{\rm Helm}_{\rm rms} = \sqrt{R_d^2 + 5\sigma^2} \, . \tag{23}$$

From these definitions we construct the following neutron-proton radius differences that will be used:

$$\Delta R_d = R_d(n) - R_d(p) \, , \tag{24}$$

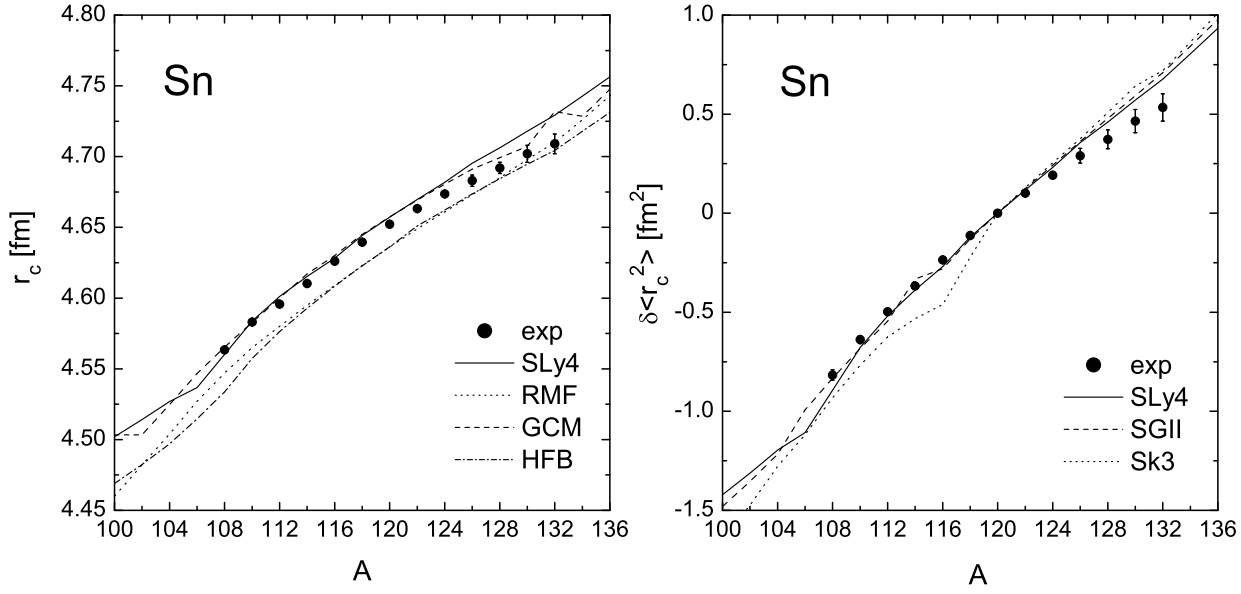

FIGURE 1. Left panel: Charge rms radii r_c of tin isotopes. The SLy4 result is compared with the results from RMF calculations [11], HFB [10] and GCM [10]. Experimental data are from [38, 39, 40, 41]; Right panel: Theoretical (with different Skyrme forces) and experimental isotope shifts $\delta\langle r_c^2\rangle$ of tin isotopes relative to ^{120}Sn.

$$\Delta R_{\rm hs} = R_{\rm hs}(n) - R_{\rm hs}(p) = \sqrt{5/3}\left[< r_n^2 >^{1/2} - < r_p^2 >^{1/2}\right], \tag{25}$$

$$\Delta R_{\rm Helm} = R_{\rm Helm}(n) - R_{\rm Helm}(p). \tag{26}$$

Beginning with Sn isotopes for which more data and calculations are available, we show on the right panel of Fig. 1 our results for the squared charge radii differences in Sn isotopes obtained from three different Skyrme forces, SLy4, SGII and Sk3. We compare them to experiment, taking the radius of ^{120}Sn as the reference [41]. On the left panel we compare our SLy4 results for the charge radii with the other theoretical approaches mentioned above. The general purpose of Fig. 1 is firstly to show that different Skyrme forces do not differ much in their predictions of the charge rms radii and secondly, to show that our results with SLy4 are comparable to other theoretical predictions including approaches that go beyond the mean-field approximation, as well as relativistic approaches. We conclude that our method reproduces the experimental data with a similar accuracy to other microscopic calculations that, as explained above, may be more sophisticated but may also be more time consuming. This agreement provides a good starting point to make predictions for other quantities such as neutron-proton radii differences, where the experimental information is scarce and it is not as accurate as in the case of charge radii.

In Fig. 2 we plot the differences between the rms of neutrons and protons $\Delta r_{np} = r_n - r_p$. On the left panel we show our results for Sn isotopes and compare them to RMF results and to experimental data. As we can see the experimental data are located between the predictions of both theoretical approaches and in general, there is agreement with experiment within the error bars. On the right panels we see the predictions for Δr_{np} in the cases of Ni and Kr isotopes, where there are no data. As it can be seen, the RMF results for the difference Δr_{np} systematically overestimate the Skyrme HF results. The reason for this is related to the difference in the nuclear symmetry energy and, consequently, to the different neutron EOS which has been extensively studied in recent years [25, 26, 58, 59].

Figure 3 shows the neutron (solid) and proton (dashed) densities $\rho_0(R)$ (8) in the ^{100,120,136}Sn isotopes. From left to right we see the evolution of these densities with the increase of the number of neutrons. In the case of ^{100}Sn (N=Z=50) we see that the two densities are practically the same except for Coulomb effects that make the protons to be more extended and, therefore, this has to be compensated with a small depression in the interior. The effect of adding more and more neutrons is to populate and extend the neutron densities. This makes also the proton distribution to follow the neutron one, increasing its spatial extension. The cost of this radius enlargement in the case of protons is a depression in the nuclear interior to preserve the normalization to the constant number of protons $Z = 50$. Then, it can be seen graphically the emergence of a region at the surface where the protons have practically disappeared while the neutrons still survive. We will quantify later this region in terms of the neutron skin thickness definitions.

The thickness of a neutron skin in nuclei may be defined in different ways. One of these possibilities is to define it as the difference between the root mean square radius of neutrons and that of protons, as we have plotted in Fig. 2. Similarly, it can be defined as the difference between the neutron and proton radii of the equivalent uniform spheres

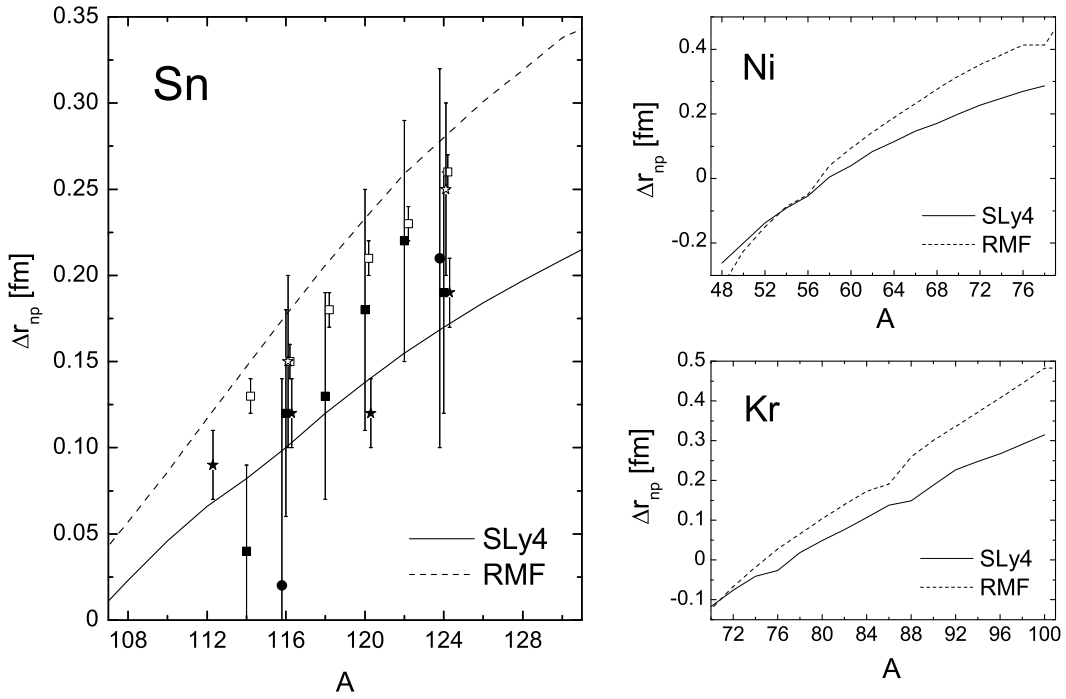

FIGURE 2. Difference between neutron and proton rms radii Δr_{np} of Sn, Ni, and Kr isotopes calculated with SLy4 force. The RMF calculation results are from Ref. [11]. The experimental data for Sn isotopes measured in (p, p) reaction (open stars) [1, 2], antiproton atoms (full stars) [3], giant dipole resonance method (full circles) [7] and spin dipole resonance method (full and open squares) [8, 9] are also shown.

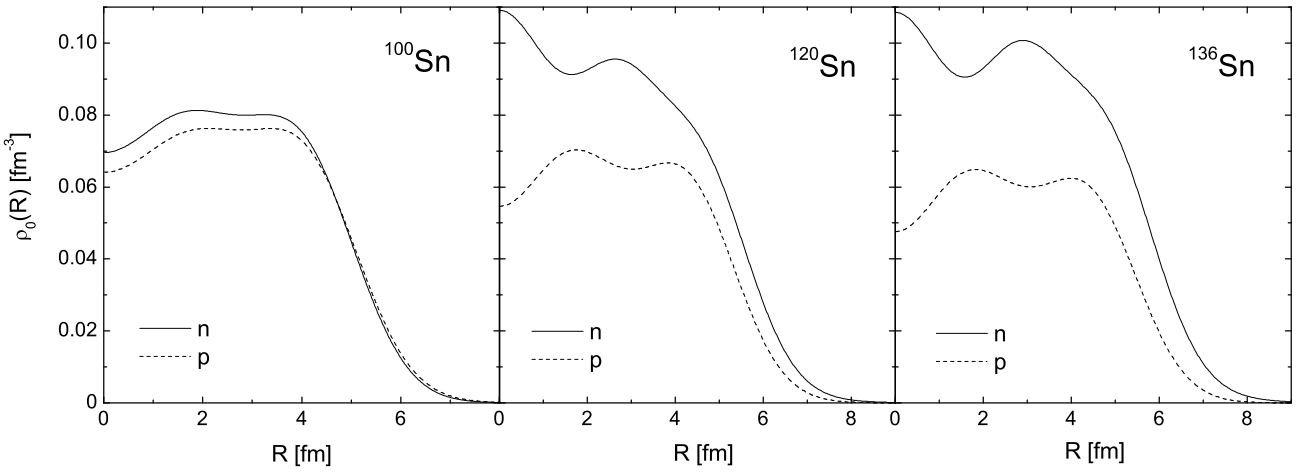

FIGURE 3. HF+BCS proton and neutron densities $\rho_0(R)$ of ^{100}Sn, ^{120}Sn, and ^{136}Sn calculated with SLy4 force.

[Eq. (25)]. Alternatively, it can be defined as the difference between the neutron and proton diffraction radii (24) or Helm radii (26).

On the other hand, the skin thickness can be also defined in terms of some criteria that the neutron and proton densities must fulfill. In Ref. [13] the neutron skin thickness is defined as the difference between two radii, R_1 and R_2, where R_1 is the radius at which the ratio of the neutron density to the proton density is equal to some given value (4 in [13]) and R_2 is the radius at which the neutron density becomes smaller than some percentage of the density at the center of the nucleus (1 % in [13]). When this difference, $\Delta R = R_2 - R_1$, is larger than some established value (in [13] this value is 1 fm, which is comparable to the range of the nuclear force), a neutron skin with skin thickness ΔR is said to occur. We have also considered the case where the first criterion for the inner radius R_1 of the neutron skin is changed. We use instead of the above criterion for R_1, the radius at which the proton density becomes smaller than 1% of the latter at the center, which is similar to the criterion used to define the outer radius R_2, but in this case for proton density instead of the neutron density. When we use the conditions in Ref. [13], we call it criterion (a). When we use the alternative condition for R_1, we call it criterion (b).

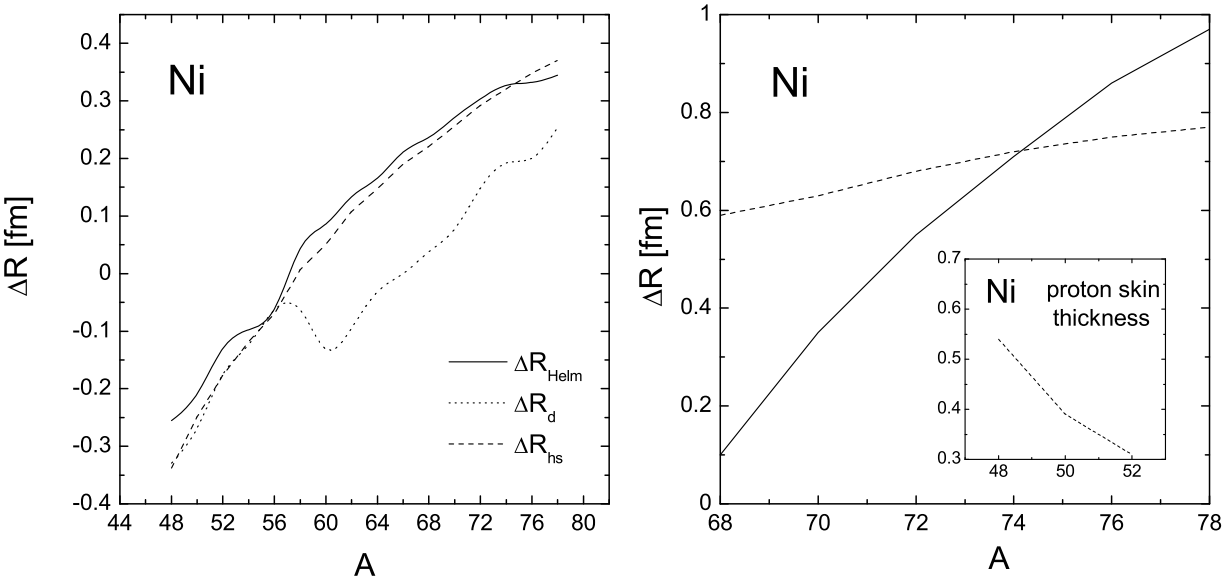

FIGURE 4. Neutron skin thicknesses for Ni isotopes. Left panel: $\Delta R_{\rm d}$ [Eq. (24)], $\Delta R_{\rm hs}$ [Eq. (25)], and $\Delta R_{\rm Helm}$ [Eq. (26)]; Right panel: corresponding to criterion (a) (solid line) and criterion (b) (dotted line). A formation of proton skin thickness with the criterion (b) is also shown.

We show in Fig. 4 the results obtained for the neutron skin thickness in Ni isotopes according to the different definitions discussed above. The left panel contains the results for definitions involving directly the difference between neutron and proton radii [Eqs. (24)-(26)]. The skin thickness predicted by the difference of the diffraction radii is in general smaller than the thickness predicted by the other two more involved options that are very similar in this range of masses. The right panel contains the neutron skin thickness defined according to the criteria on the density distributions (a) (solid line) and (b) (dashed line). They only differ in the way in which the starting radius of the skin R_1 is chosen. One can see that we obtain larger neutron skin thicknesses when using criterion (b) in the lighter isotopes, but this is reversed for heavier isotopes and we get larger thickness when using criterion (a).

We also consider the most neutron-deficient region of Ni isotopes in a search for the formation of a proton skin. Reversing the definitions of R_1 and R_2 and applying the criterion (b) with protons and neutrons interchanged, the obtained results are shown in the inset of the right panel in Fig. 4. We find no proton skin when applying criterion (a). One can see that a small skin starts developing in these isotopes but we cannot push it further because ^{48}Ni is already at the proton drip line. The results are then not conclusive enough to assess the existence of a proton skin in these isotopes.

When the nucleus is deformed, the thickness of the neutron skin might depend on the direction. It is an interesting and natural question to ask whether the deformed densities give rise to a different skin size in the different directions. It is also interesting to know whether the emergence of the skin may be influenced by the nuclear shape. We first study the intrinsic density distributions $\rho(\vec{R})$ in various selected directions. For that purpose we show in Figs. 5 and 6 the densities of ^{98}Kr for oblate and prolate shapes, respectively. We can see the spatial distributions for neutrons (solid) and protons (dotted) in three different directions: z-direction $(r = 0)$, r-direction $(z = 0)$, and $r = z$ direction. We can observe that the profiles of the densities as well as the spatial extensions change with the direction. Clearly, the densities are more extended in the z-direction in the case of prolate shapes. The opposite is true in the case of oblate shapes. The case $r = z$ gives always intermediate densities. We have added in the three directions a couple of full dots, indicating the radii R_1 and R_2 that defines the skin thickness according to the above mentioned criterion (a).

It is also worth looking at the points in the (r,z) plane that define the ellipses where the criteria for R_1 and R_2 are met. Figure 7 shows these points for protons (thin lines) and neutrons (thick lines) and for the two shapes, prolate (solid) and oblate (dashed). We can see that the size of the skin changes little with the directions perpendicular to the surface, but shows a tendency to increase on the shorter axis. It is interesting to note that the skin size of the spherical component $\rho_0(R)$ is an intermediate value. The overall skin thickness is also similar in the oblate and prolate equilibrium shapes. From this example we may conclude that the skin thickness does not depend much on the oblate or prolate character of the deformation.

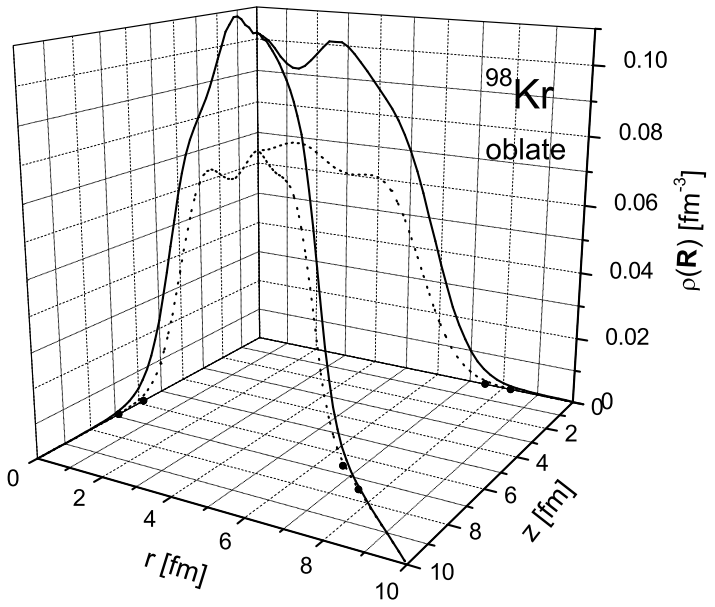

FIGURE 5. Neutron (solid line) and proton (dotted line) density distributions $\rho(\vec{R})$ in different directions for oblate shape of ^{98}Kr. The full dots shown on the (r,z) plane correspond to radii R_1 and R_2 according to criterion (a).

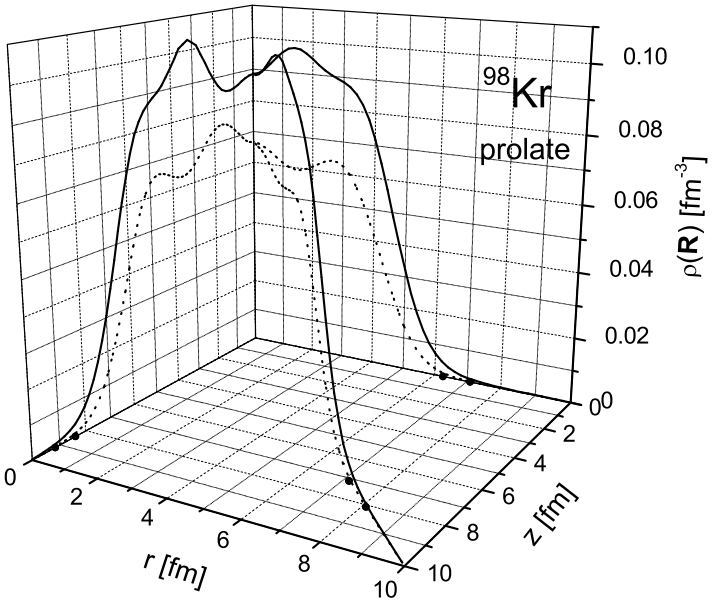

FIGURE 6. Same as in Fig. 5, but for prolate shape of ^{98}Kr.

SYMMETRY ENERGY AND SURFACE PROPERTIES OF NEUTRON-RICH EXOTIC NUCLEI

The symmetry energy $S(\rho)$ is related to the Taylor series expansion of the energy per particle for nuclear matter (NM) in terms of the isospin asymmetry $\delta = (\rho_n - \rho_p)/\rho$

$$E(\rho,\delta) = E(\rho,0) + S(\rho)\delta^2 + O(\delta^4) + \cdots \ , \tag{27}$$

where $\rho = \rho_n + \rho_p$ is the baryon density with ρ_n and ρ_p denoting the neutron and proton densities, respectively (see, e.g. [58, 60]). Odd powers of δ are forbidden by the isospin symmetry and the terms proportional to δ^4 and higher orders are found to be negligible.

Near the saturation density ρ_0 the energy of isospin-symmetric matter, $E(\rho,0)$, and the symmetry energy, $S(\rho)$, can be expanded as

$$E(\rho,0) = E_0 + \frac{K}{18\rho_0^2}(\rho-\rho_0)^2 + \cdots \ , \tag{28}$$

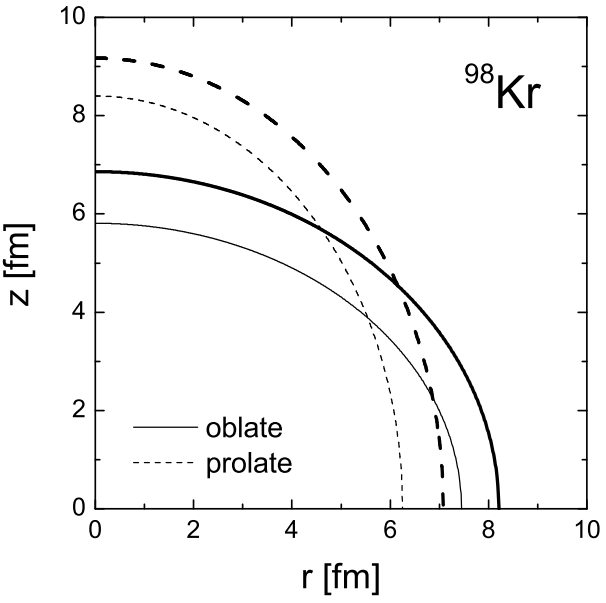

FIGURE 7. Radii R_1 and R_2 according to criterion (a) for neutrons (thick lines) and protons (thin lines) in ^{98}Kr nucleus (shown in rz plane) corresponding to its oblate (solid lines) and prolate (dashed lines) shape.

and

$$S(\rho) = \frac{1}{2}\left.\frac{\partial^2 E(\rho,\delta)}{\partial\delta^2}\right|_{\delta=0} = a_4 + \frac{p_0}{\rho_0^2}(\rho-\rho_0) + \frac{\Delta K}{18\rho_0^2}(\rho-\rho_0)^2 + \cdots . \tag{29}$$

The parameter a_4 is the symmetry energy at equilibrium ($\rho=\rho_0$). The pressure p_0^{NM}

$$p_0^{NM} = \rho_0^2\left.\frac{\partial S}{\partial\rho}\right|_{\rho=\rho_0} \tag{30}$$

and the curvature ΔK^{NM}

$$\Delta K^{NM} = 9\rho_0^2\left.\frac{\partial^2 S}{\partial\rho^2}\right|_{\rho=\rho_0} \tag{31}$$

of the nuclear symmetry energy at ρ_0 govern its density dependence and thus provide important information on the properties of the nuclear symmetry energy at both high and low densities. The widely used "slope" parameter L^{NM} is related to the pressure p_0^{NM} [Eq. (30)] by

$$L^{NM} = \frac{3p_0^{NM}}{\rho_0}. \tag{32}$$

The CDFM was suggested and developed in Refs. [47, 48, 49]. The model is related to the delta-function limit of the generator coordinate method [48, 49, 61]. In the model the one-body density matrix (OBDM) $\rho(\mathbf{r},\mathbf{r}')$ is written as a coherent superposition of the OBDM's for spherical "pieces" of nuclear matter $\rho_x(\mathbf{r},\mathbf{r}')$ (so-called "fluctons") with density $\rho_x(\mathbf{r}) = \rho_0(x)\Theta(x-|\mathbf{r}|)$ with $\rho_0(x) = 3A/(4\pi x^3)$:

$$\rho(\mathbf{r},\mathbf{r}') = \int_0^\infty dx|\mathscr{F}(x)|^2\rho_x(\mathbf{r},\mathbf{r}') \tag{33}$$

with

$$\rho_x(\mathbf{r},\mathbf{r}') = 3\rho_0(x)\frac{j_1(k_F(x)|\mathbf{r}-\mathbf{r}'|)}{(k_F(x)|\mathbf{r}-\mathbf{r}'|)}\Theta\left(x-\frac{|\mathbf{r}+\mathbf{r}'|}{2}\right). \tag{34}$$

The generator coordinate x is the radius of a sphere containing Fermi gas of all A nucleons uniformly distributed in it. In Eq. (34) j_1 is the first-order spherical Bessel function and

$$k_F(x) = \left(\frac{3\pi^2}{2}\rho_0(x)\right)^{1/3} \equiv \frac{\alpha}{x} \tag{35}$$

with

$$\alpha = \left(\frac{9\pi A}{8}\right)^{1/3} \simeq 1.52A^{1/3} \tag{36}$$

is the Fermi momentum of such a formation.

In the CDFM the Wigner distribution function which corresponds to the OBDM from Eq. (33) is:

$$W(\mathbf{r},\mathbf{k}) = \int_0^\infty dx|\mathscr{F}(x)|^2 W_x(\mathbf{r},\mathbf{k}), \tag{37}$$

where

$$W_x(\mathbf{r},\mathbf{k}) = \frac{4}{(2\pi)^3}\Theta(x-|\mathbf{r}|)\Theta(k_F(x)-|\mathbf{k}|). \tag{38}$$

Correspondingly to $W(\mathbf{r},\mathbf{k})$ from Eq. (37), the density $\rho(\mathbf{r})$ in the CDFM is expressed by means of the same weight function $|\mathscr{F}(x)|^2$:

$$\rho(\mathbf{r}) = \int d\mathbf{k} W(\mathbf{r},\mathbf{k}) = \int_0^\infty dx|\mathscr{F}(x)|^2 \frac{3A}{4\pi x^3}\Theta(x-|\mathbf{r}|) \tag{39}$$

normalized to the mass number:

$$\int \rho(\mathbf{r}) d\mathbf{r} = A. \tag{40}$$

If one takes the delta-function approximation to the Hill-Wheeler integral equation in the generator coordinate method one gets a differential equation for the weight function $\mathscr{F}(x)$ [48, 49, 61]. Instead of solving this differential equation we adopt a convenient approach to the weight function $|\mathscr{F}(x)|^2$ proposed in Refs. [47, 48, 49]. In the case of monotonically decreasing local densities (*i.e.* for $d\rho(r)/dr \leq 0$), the latter can be obtained by means of a known density distribution $\rho(r)$ for a given nucleus:

$$|\mathscr{F}(x)|^2 = -\frac{1}{\rho_0(x)} \left.\frac{d\rho(r)}{dr}\right|_{r=x}. \tag{41}$$

The normalization of the weight function is:

$$\int_0^\infty dx|\mathscr{F}(x)|^2 = 1. \tag{42}$$

Considering the pieces of nuclear matter with density $\rho_0(x)$ one can use for the matrix element $V(x)$ of the nuclear Hamiltonian the corresponding nuclear matter energy from the method of Brueckner *et al.* [45, 46]. In this energy-density method the expression for $V(x)$ reads

$$V(x) = AV_0(x) + V_C - V_{CO}, \tag{43}$$

where

$$\begin{aligned} V_0(x) &= 37.53[(1+\delta)^{5/3} + (1-\delta)^{5/3}]\rho_0^{2/3}(x) + b_1\rho_0(x) + b_2\rho_0^{4/3}(x) + b_3\rho_0^{5/3}(x) \\ &+ \delta^2[b_4\rho_0(x) + b_5\rho_0^{4/3}(x) + b_6\rho_0^{5/3}(x)] \end{aligned} \tag{44}$$

with $b_1 = -741.28$, $b_2 = 1179.89$, $b_3 = -467.54$, $b_4 = 148.26$, $b_5 = 372.84$, and $b_6 = -769.57$. $V_0(x)$ in Eq. (43) corresponds to the energy per nucleon in nuclear matter (in MeV) with the account for the neutron-proton asymmetry. V_C is the Coulomb energy of protons in a "flucton" and V_{CO} is the Coulomb exchange energy. Thus, in the Brueckner EOS [Eq. (44)], the potential symmetry energy turns out to be proportional to δ^2. Only in the kinetic energy the dependence on δ is more complicated. Substituting $V_0(x)$ in Eq. (29) and taking the second derivative, the symmetry energy $S^{NM}(x)$ of the nuclear matter with density $\rho_0(x)$ (the coefficient a_4 in Eq. (29)) can be obtained:

$$S^{NM}(x) = 41.7\rho_0^{2/3}(x) + b_4\rho_0(x) + b_5\rho_0^{4/3}(x) + b_6\rho_0^{5/3}(x). \tag{45}$$

The corresponding analytical expressions for the pressure $p_0^{NM}(x)$ and asymmetric compressibility $\Delta K^{NM}(x)$ of such a system in the Brueckner theory have the form:

$$p_0^{NM}(x) = 27.8\rho_0^{5/3}(x) + b_4\rho_0^2(x) + \frac{4}{3}b_5\rho_0^{7/3}(x) + \frac{5}{3}b_6\rho_0^{8/3}(x) \tag{46}$$

and

$$\Delta K^{NM}(x) = -83.4\rho_0^{2/3}(x) + 4b_5\rho_0^{4/3}(x) + 10b_6\rho_0^{5/3}(x). \tag{47}$$

Under some approximation in the CDFM the symmetry energy, the slope and the curvature for finite nuclei are obtained as infinite superpositions of the corresponding quantities of nuclear matter (with a given density $\rho_0(x)$) weighted by means of the function $|\mathscr{F}(x)|^2$:

$$s = \int_0^\infty dx|\mathscr{F}(x)|^2 S^{NM}(x), \tag{48}$$

$$p_0 = \int_0^\infty dx|\mathscr{F}(x)|^2 p_0^{NM}(x), \tag{49}$$

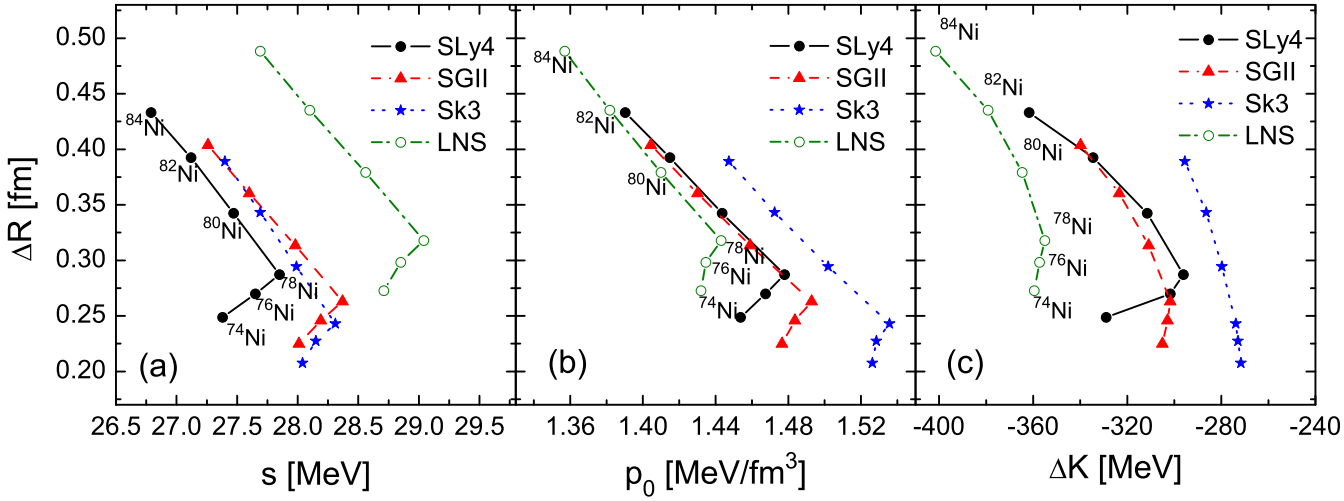

FIGURE 8. HF+BCS neutron skin thicknesses ΔR for Ni isotopes as a function of the symmetry energy s (a), pressure p_0 (b), and asymmetric compressibility ΔK (c) calculated with SLy4, SGII, Sk3, and LNS forces.

$$\Delta K = \int_0^\infty dx |\mathscr{F}(x)|^2 \Delta K^{NM}(x). \tag{50}$$

The symmetry energy, the pressure and the asymmetric compressibility are calculated within the CDFM according to Eqs. (48)-(50) by using the weight functions (41) calculated from the self-consistent HF+BCS densities [33] with different Skyrme force parametrizations.

The main emphasis of our study is to inspect the correlation of the neutron skin thickness $\Delta R = \Delta r_{np} = r_n - r_p$ of nuclei in a given isotopic chain with the s, p_0 and ΔK parameters extracted from the density dependence of the symmetry energy around the saturation density. We show first in Fig. 8 the results for Ni isotopes. It is seen from Fig. 8(a) that there exists an approximate linear correlation between ΔR and s for the even-even Ni isotopes with A=74-84. We observe a smooth growth of the symmetry energy till the double-magic nucleus ^{78}Ni (N=50) and then a linear decrease of s while the neutron skin thickness of the isotopes increases. This behavior is valid for all Skyrme parametrizations used in the calculations, in particular, the average slope of ΔR for various forces is almost the same. The LNS force yields larger values of s comparing to the other three Skyrme interactions. In this case the small deviation can be attributed to the fact that the LNS force has not been fitted to finite nuclei and therefore, one cannot expect a good quantitative description at the same level as purely phenomenological Skyrme forces. As a consequence, the neutron skin thickness calculated with LNS force has a larger size with respect to the other three forces whose results for ΔR are comparable with each other.

The analysis of the correlation between the neutron skin thickness and some macroscopic nuclear matter properties in finite nuclei is continued by showing the results for a chain of Sn isotopes. This is done in Fig. 9, where the results obtained with SLy4, SGII, Sk3, and LNS Skyrme forces are presented for isotopes with A=124-152. Similarly to the case of Ni isotopes with transition at specific shell closure, we observe a smooth growth of the symmetry energy till the double-magic nucleus ^{132}Sn (N=82) and then an almost linear decrease of s while the neutron skin thickness of the isotopes increases. In Ref. [29] we have studied a formation of a neutron skin in tin isotopes with smaller A where very poor experimental information is available. For instance, a large uncertainty is shown to exist experimentally in the neutron skin thickness of ^{124}Sn, i.e., its value varies from 0.1 to 0.3 fm depending on the experimental method. Our theoretical prediction ΔR=0.17 fm for this nucleus is found to be within the above experimental band. A similar approximate linear correlation between ΔR and p_0 for Sn isotopes is also shown in Fig. 9(b). The asymmetric compressibility ΔK given in Fig. 9(c) is less correlated than p_0 with ΔR within the Sn isotopic chains.

An illustration of a possible correlation of the neutron-skin thickness ΔR with the s and p_0 parameters extracted from the density dependence of the symmetry energy around the saturation density for the Kr isotopic chain is given in Fig. 10. It can be seen from Fig. 10 that there exists an approximate linear correlation between ΔR and s for the even-even Kr isotopes with A=82-96. Similarly to the behavior of ΔR vs s dependence for the cases of Ni and Sn isotopes shown in Figs. 8 and 9, respectively, we observe a smooth growth of the symmetry energy up to the semi-magic nucleus ^{86}Kr (N=50) and then a linear decrease of s while the neutron-skin thickness of the isotopes increases. This linear tendency expressed for Kr isotopes with $A > 86$ is similar for the cases of both oblate and prolate deformed shapes. We note that all Skyrme parametrizations used in the calculations reveal similar behavior; in particular, the average slope of ΔR for various forces is almost the same. In addition, one can see from Fig. 10 a stronger deviation between the results for oblate and prolate shape of Kr isotopes in the case of SGII parametrization when displaying the correlation between ΔR and s. This is valid also for the correlation between ΔR and p_0, where more distinguishable results for both types of deformation are present. The neutron skin thickness ΔR for Kr isotopes correlates with p_0 almost linearly, as in the symmetry-energy

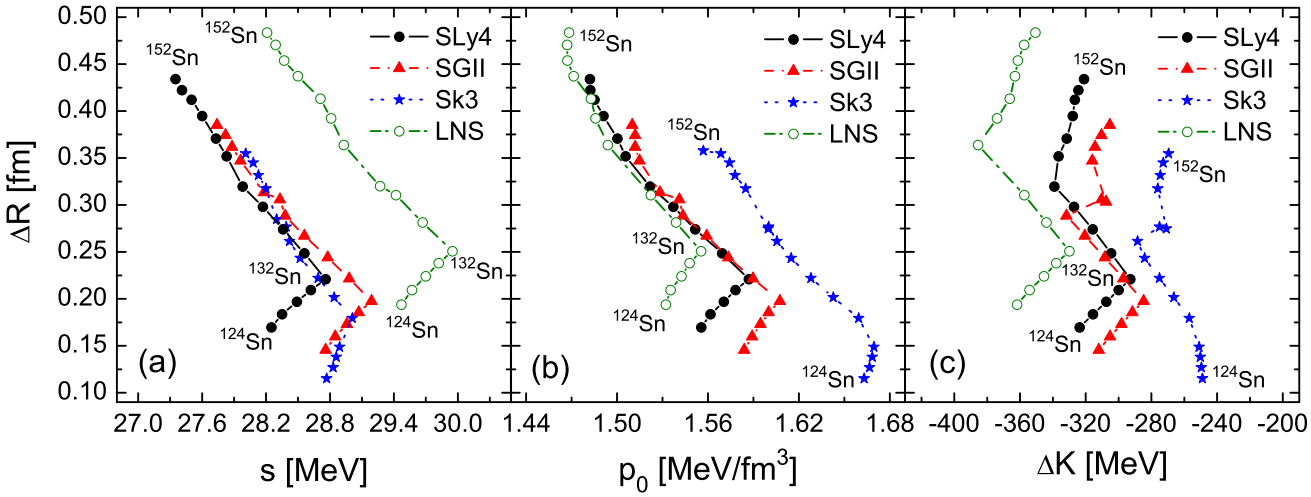

FIGURE 9. Same as in Fig. 8, but for Sn isotopes.

case, with an inflexion point transition at the semi-magic ^{86}Kr nucleus. In addition, one can see also from Fig. 10 that the calculated values for p_0 are smaller in the case of LNS and SLy4 forces than for the other two Skyrme parameter sets. In general, we would like to note that the behavior of deformed Kr isotopes shown in Fig. 10 is comparable with the one found for the spherical Ni and Sn isotopes having a magic proton number. The small differences just indicate that stability patterns are less regular within isotopic chains with a non-magic proton number.

As a general discussion of the results shown in Figures 8, 9, and 10 we would like to note that the growth of the symmetry energy with the increase of the mass number for a given isotopic chain up to the double-magic nuclei followed by its decrease is related to the fact that, in particular, for a stiff symmetry energy, it is favorable to push the excess neutrons to the surface where the symmetry energy is small. In other words, the strong correlation of the neutron-skin thickness of heavy nuclei with the density dependence of the symmetry energy is a result of the dynamical competition between the surface tension and the difference between the symmetry energy at the center and surface of the nucleus.

The theoretical neutron skin thickness ΔR of Pb nuclei (A=202–214) against the parameters of interest, s, p_0, and ΔK, is illustrated in Fig. 11. All predicted correlations manifest an almost linear dependence and no pronounced kink at ^{208}Pb is observed. Similarly to all isotopes presented in this study, the LNS force produces larger symmetry energies s than the other three forces also for Pb nuclei with values exceeding 30 MeV. Another peculiarity of the results obtained with LNS is the almost constant ΔK observed in Fig. 11a.

Further attention deserves the value of the neutron skin thickness in ^{208}Pb, whose determination has motivated recent experiments. The model-independent measurement of parity-violating asymmetry (which is sensitive to the neutron distribution) in the elastic scattering of polarized electrons from ^{208}Pb at JLAB within the PREX Collaboration [51, 52] has provided the first electroweak observation of ΔR=$0.33^{+0.16}_{-0.18}$ fm in ^{208}Pb. Obviously, future precise measurements are needed to reduce the quoted uncertainties of ΔR. The distorted wave electron scattering calculations for ^{208}Pb [55] extracted a result for the neutron skin thickness which agrees with that reported in the experimental paper [52]. The value of ΔR for ^{208}Pb (0.1452 fm) deduced from the present HF+BCS calculations with SLy4 force agrees with the recent experimentally extracted skin thickness ($0.156^{+0.025}_{-0.021}$ fm) using its correlation with the dipole polarizability [53]. However, this experimental value was derived by means of covariance analysis based on one Skyrme functional (SV-min). In this respect, a systematic study with a variety of EDFs as well as experimental tests in other nuclei would be important because the correlation between polarizability, neutron skin thickness, and symmetry energy is model-dependent (see, for example, Fig. 1 of Ref. [57]). In addition, our theoretically obtained value of ΔR for ^{208}Pb agrees well with the value 0.18 ± 0.027 fm from Ref. [62]. It is lower than the one obtained in Refs. [25] and [28] with the same Skyrme force, but is in agreement with the values calculated with self-consistent densities of several nuclear mean-field models (see Table I in Ref. [63]). The p_0 and ΔK values for ^{208}Pb are in a good agreement with those from Ref. [25].

Following the analysis within the CDFM approach [30], we give (e.g., in Ref. [31]) more detailed study of the weight function $|\mathscr{F}(x)|^2$ (that is related to the density and thus, to the structural peculiarities) to understand the kinks observed in the relationships between ΔR and s, as well as ΔR and p_0. The latter were shown to exist [30] in double-magic nuclei in the cases of Ni (at ^{78}Ni) and Sn (at ^{132}Sn) isotopic chains. As one can see in Fig. 10 of the present work, they exist also in the considered cases of Kr (at ^{86}Kr) isotopes. In contrast, such a kink does not exist in the case of Pb isotopic chain (at ^{208}Pb, particularly). Here we would like only to analyze the quantity

$$\Delta s_{\pm} = \frac{s_{A\pm2} - s_A}{s_A} \tag{51}$$

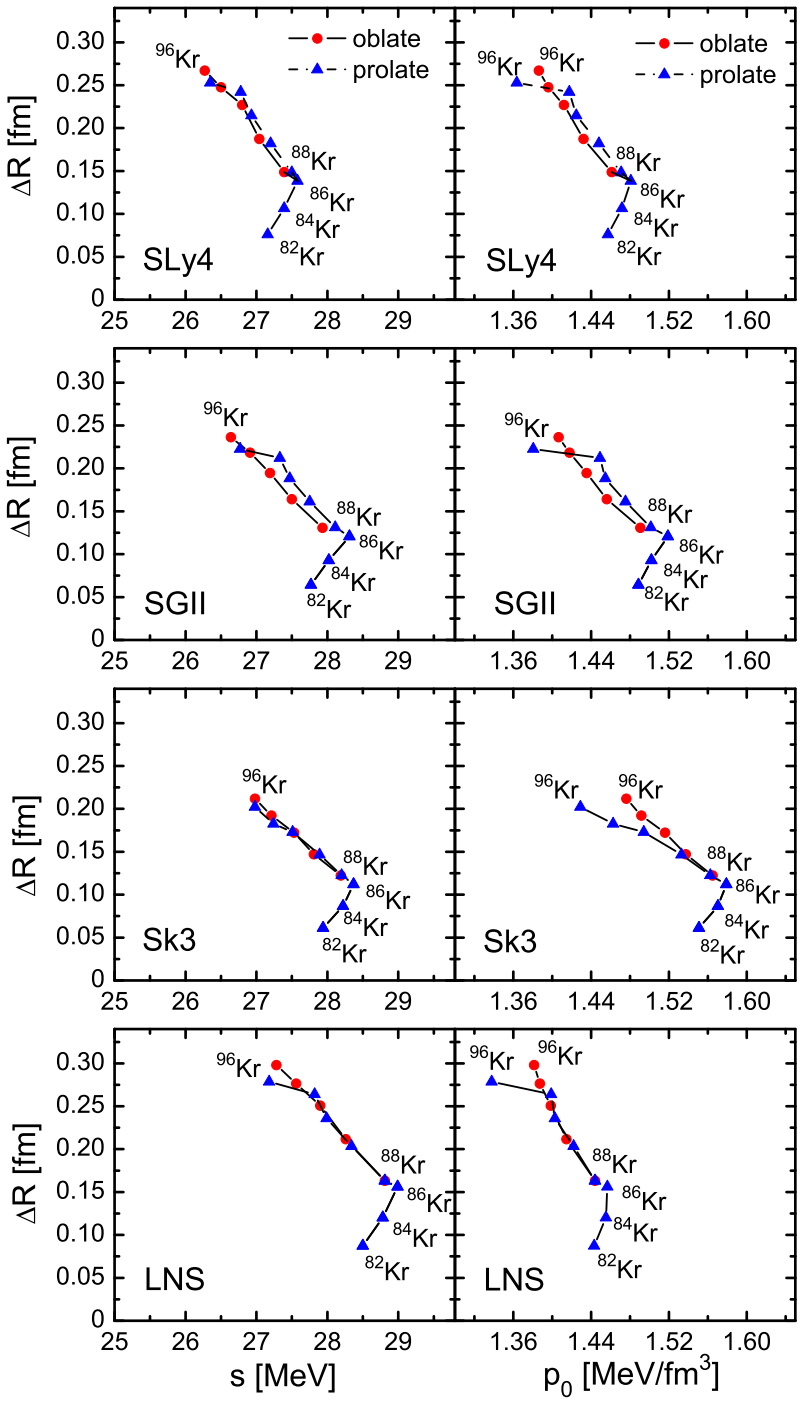

FIGURE 10. HF+BCS neutron skin thicknesses ΔR for Kr isotopes as a function of the symmetry energy s and the pressure p_0 calculated with SLy4, SGII, Sk3, and LNS forces and for oblate and prolate shapes. The results for oblate and prolate shape for $A = 82, 84$ isotopes are indistinguishable.

that is a direct measure of the relative deviation of the symmetry energy with respect to the double-magic nuclei taking them as reference nuclei in each of the chains, where the kinks are expected. The values of Δs_+ and Δs_- are listed in Table 1, where the two numbers for each isotopic chain correspond to the range of integration Δx that contains the peak of $|\mathscr{F}(x)|^2$ [31]. One can see first from this Table that the absolute values of Δs_+ and Δs_- for Pb isotopes are comparable with each other, which is not the case for the two other isotopic chains. Second, and very important is that the Δs_+ value turns out to be negative and Δs_- value to be positive for Pb isotopes at the range of integration Δx, and this is the main difference regarding to the corresponding values (both are negative) in the Ni and Sn chains.

These differences can be attributed to the profiles of the density distributions, particularly in the surface region. Their monopole components $\rho_0(R)$ (coming from the density multipole expansion) are given in Fig. 12, where curves for five Ni, Sn, Pb isotopes around double-magic ^{78}Ni, ^{132}Sn, and ^{208}Pb nuclei are presented in panels (a), (b), and (c),

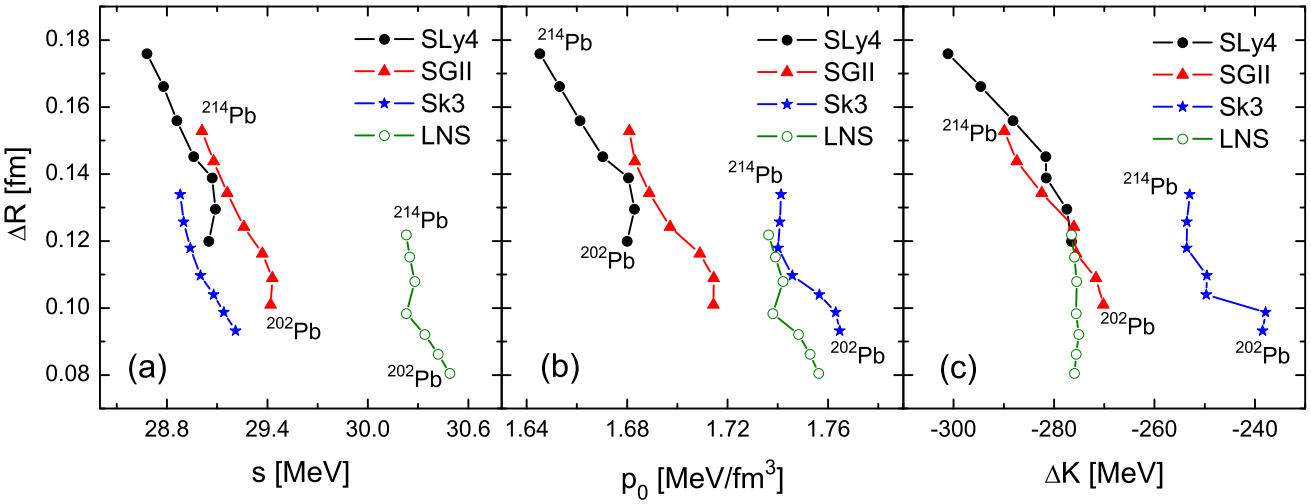

FIGURE 11. HF+BCS neutron skin thicknesses ΔR for Pb isotopes as a function of the symmetry energy s (a), pressure p_0 (b), and asymmetric compressibility ΔK (c) calculated with SLy4, SGII, Sk3, and LNS force.

TABLE 1. Relative deviation values of the symmetry energy Δs_+ and Δs_- [Eq. (51)] for the range of integration Δx in Eq. (48) and for Ni, Sn, and Pb isotopes.

	Ni	Sn	Pb
Δs_+	-0.0137	-0.0070	-0.0035
Δs_-	-0.0072	-0.0049	0.0038

respectively. One can see from Fig. 12 the same trend in the tails of the three isotopic chains, which are ordered according to the mass number A, being higher for heavier isotopes to produce larger radii. On the other hand the behavior in the top part of the surface region, shown in the inset of the panels, is different. In the case of Ni and Sn isotopes in panels (a) and (b), one observes that the double-magic nuclei have the largest density with all the neighboring isotopes lying below. In the case of Pb isotopes in panel (c), the density increases from heavier to lighter isotopes with the double-magic nucleus in between. In Pb isotopes, this ordering is opposite in the tail. As a result of this, the slope of the density in Pb isotopes, and therefore $|\mathscr{F}(x)|^2$, decreases with the number of neutrons continuously and no kink is present in the symmetry energy. On the other hand, in the case of Ni and Sn isotopes, the slope of the density is larger for the double-magic isotopes generating a kink in the symmetry energy.

SUMMARY

In the present work we review results of our studies on some important properties of neutron-rich exotic nuclei mainly related with the nuclear surface and characterized by a skin emergence and quantities coming from the density dependence of the nuclear symmetry energy.

For a first time the various definitions which have been previously proposed to determine the neutron skin thickness, involving both matter radii and tails of nuclear densities, have been compared within a deformed Skyrme HF+BCS model. Three Skyrme parametrizations have been involved in the calculations: SGII, Sk3 and SLy4. Most of the results shown in the paper are obtained with SLy4 force, but the other Skyrme interactions produce similar results. We found that all definitions of the neutron skin predict to a different extent the existence of a skin in nuclei far from the stability line. Particularly, a pronounced neutron skin can be attributed to heavier isotopes of the three chains considered, namely with $A > 132$ for Sn, $A > 74$ for Ni, and $A > 96$ for Kr isotopes. We also found that for a given isotopic chain the increase of the skin with the neutron number in the neutron-rich nuclei exhibits a rather constant slope, which is different depending on the definition of nuclear skin. More significant neutron skin is obtained when analyzing its formation by means of definition from Ref. [13] (called criterion (a)) or using an alternative one (called criterion (b)). In this case we get an absolute size of the skin larger than 0.4 fm and almost reaching 1 fm for the heaviest isotopes (in the case of criterion (a)). At the same time, the neutron skin determined by the difference between neutron and proton radii using diffraction parameters defined in the Helm model shows a more smooth gradual increase with the neutron excess and it is in size of around 0.3–0.4 fm.

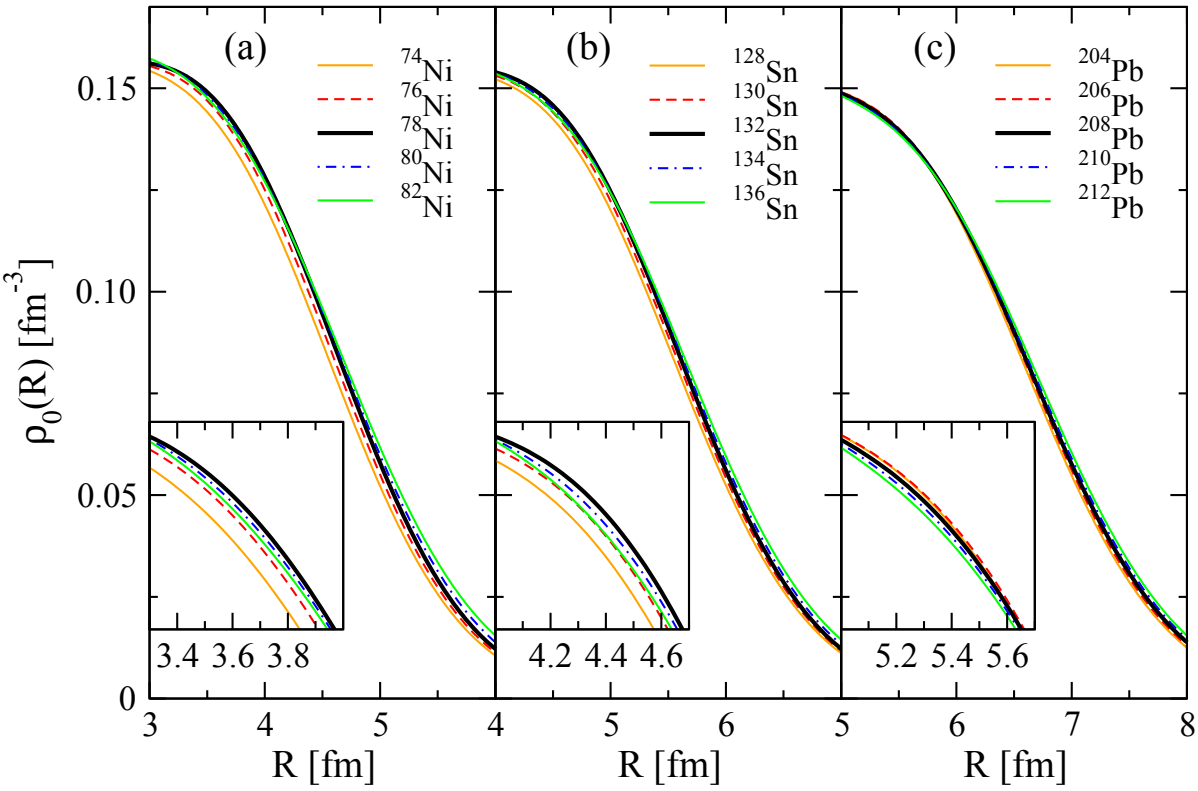

FIGURE 12. HF+BCS total densities in the surface region for five Ni (A=74–82) isotopes (a), five Sn (A=128–136) isotopes (b), and five Pb (A=204–212) isotopes (c) around double-magic ^{78}Ni, ^{132}Sn, and ^{208}Pb nuclei, respectively, calculated with SLy4 force.

We also show on the example of the neutron-deficient Ni isotopes the possibility to find a proton skin in a similar way to the neutron skin. Although the analysis, which was performed in our paper for this case, uses an alternative criterion to that applied in [13], it indicates a situation close to proton skin formation in Ni isotopes very close to the proton drip line. However, the search for the existence of proton skin could be explored in the most proton-rich nuclei approaching the proton drip lines of lighter nuclei, where $Z > N$.

In the present work the effects of deformation on the skin formation are studied in Kr isotopes which are well deformed nuclei. Taking as an example ^{98}Kr and ^{100}Kr isotopes, we found that the profiles of the proton and neutron densities, as well as the spatial extensions change with the direction in both oblate and prolate shapes. At the same time, the neutron skin thickness remains almost equal along the different directions perpendicular to the surface. We found out a very weak dependence of the neutron skin formation on the character of deformation.

A theoretical approach to the nuclear many-body problem combining the deformed HF+BCS method with Skyrme-type density-dependent effective interactions and the CDFM has been used to study nuclear properties of finite nuclei. For this purpose, we examined three chains of spherical neutron-rich Ni, Sn, and Pb isotopes and two chains of deformed neutron-rich Kr and Sm isotopes, most of them being far from the stability line and representing an interest for future measurements with radioactive exotic beams. In addition to the three Skyrme parametrizations already discussed and used one more LNS Skyrme force has been involved in the calculations.

For a first time, we have demonstrated the capability of CDFM to be applied as an alternative way to make a transition from the properties of nuclear matter to the properties of finite nuclei investigating the nuclear symmetry energy s, the neutron pressure p_0 and the asymmetric compressibility ΔK in finite nuclei. This has been carried out on the base of the Brueckner energy-density functional for infinite nuclear matter. One of the advantages of the CDFM is the possibility to obtain transparent relations for the intrinsic EOS quantities analytically by means of a convenient approach to the weight function.

We have found that there exists an approximate linear correlation between the neutron skin thickness of even-even nuclei from the Ni (A=74-84), Sn (A=124-152), and Pb (A=202-214) isotopic chains and their nuclear symmetry energies. Comparing with the spherical case, we note that the linear correlation observed in the Kr (A=82-96) and Sm (A=140-156) isotopes is not smooth enough due to their different equilibrium shapes, as well as to the transition regions between them. As known, the latter are difficult to be interpreted as they exhibit a complicated interplay of competing degrees of freedom. For all classes of the considered nuclei except for the Pb isotopes an inflection point transition at specific shell closure, in particular at double-magic ^{78}Ni and ^{132}Sn nuclei and semi-magic ^{86}Kr and ^{144}Sm ones, appears for these correlations. The increase of the symmetry energy with the increase of A for a given isotopic chain until the double-magic

nuclei followed by its decrease confirms the physical interpretation given in Ref. [64], where this fact is shown to be a result from the moving of the extra neutrons to the surface thus increasing the surface tension but reducing the symmetry energy. In general, the neutron-rich skin of a heavy nucleus emerges from a dynamic competition between the surface tension and the difference between the symmetry energy at the saturation density and at a lower surface density [64].

We have analyzed in detail the existence of kinks on the example of the Ni and Sn isotopic chains and the lack of such a kink for the Pb isotopic chain. From the studies in Refs. [30, 31] and the present analysis the kinks displayed by the Ni and Sn can be understood as consequences of particular differences in the structure of these nuclei and the resulting densities and weight functions.

Concluding, we would like to note that the used microscopic theoretical methods are capable to predict the nuclear skin in exotic nuclei, as well as important quantities in finite nuclei and their relation to surface properties of these nuclei. The capability of the present methods can be further demonstrated by taking into consideration Skyrme-type and relativistic nuclear energy-density functionals. More definite conclusions on the emergence of nuclear skin can be drawn on the basis of studies of proton and neutron form factors and the related densities. Theoretical predictions for these quantities were given, e.g., in our work [50] that serve as a ground for upcoming experiments using colliding electrons with exotic nuclei in storage rings (see, e.g., Ref. [65]).

ACKNOWLEDGMENTS

E.M.G. and P.S. acknowledge support from MINECO (Spain) under Contracts No. FIS2011–23565 and No. FPA2010–17142.

REFERENCES

1. L. Ray *et al.*, Phys. Rev. C **19**, 1855 (1979).
2. G. W. Hoffmann *et al.*, Phys. Rev. Lett. **47**, 1436 (1981).
3. A. Trzcinska *et al.*, Phys. Rev. Lett. **87**, 082501 (2001).
4. T. W. Donnelly *et al.*, Nucl. Phys. **A503**, 589 (1989).
5. C. J. Horowitz *et al.*, Phys. Rev. C **47**, 826 (1993).
6. D. Vretenar, P. Finelli, A. Ventura, G. A. Lalazissis, and P. Ring, Phys. Rev. C **61**, 064307 (2000).
7. A. Krasznahorkay *et al.*, Nucl. Phys. **A567**, 521 (1994).
8. A. Krasznahorkay *et al.*, Phys. Rev. Lett. **82**, 3216 (1999).
9. A. Krasznahorkay *et al.*, Nucl. Phys. **A731**, 224 (2004).
10. J. Libert, B. Roussiere, and J. Sauvage, Nucl. Phys. **A786**, 47 (2007).
11. G. A. Lalazissis, S. Raman, and P. Ring, At. Data Nucl. Data Tables **71**, 1 (1999).
12. Z. Ren, W. Mittig, B. Chen, and Z. Ma, Phys. Rev. C **52**, R20 (1995).
13. N. Fukunishi, T. Otsuka, and I. Tanihata, Phys. Rev. C **48**, 1648 (1993).
14. R. H. Helm, Phys. Rev. **104**, 1466 (1956).
15. J. Friedrich and N. Voegler, Nucl. Phys. **A373**, 192 (1982); J. Friedrich, N. Voegler, and P.G. Reinhard, Nucl. Phys. **A459**, 10 (1986); D. W. L. Sprung, N. Yamanishi, and D. C. Zheng, Nucl. Phys. **A550**, 89 (1992).
16. S. Mizutori, J. Dobaczewski, G. A. Lalazissis, W. Nazarewicz, and P.-G. Reinhard, Phys. Rev. C **61**, 044326 (2000).
17. B. Alex Brown, Phys. Rev. Lett. **85**, 5296 (2000).
18. S. Typel and B. Alex Brown, Phys. Rev. C **64**, 027302 (2001).
19. J. L. Wood, K. Heyde, W. Nazarewicz, M. Huyse, and P. Van Duppen, Phys. Rep. **215**, 101 (1992); K. Heyde and J. L. Wood, Rev. Mod. Phys. **83**, 1467 (2011).
20. W. D. Myers and W. J. Swiatecki, Nucl. Phys. A **81**, 1 (1966).
21. P. Möller *et al.*, At. Data Nucl. Data Tables **59**, 185 (1995).
22. K. Pomorski and J. Dudek, Phys. Rev. C **67**, 044316 (2003).
23. A. Carbone, G. Colò, A. Bracco, Li-Gang Cao, P. F. Bortignon, F. Camera, and O. Wieland, Phys. Rev. C **81**, 041301(R) (2010).
24. D. Vretenar, T. Nikšić, and P. Ring, Phys. Rev. C **68**, 024310 (2003).
25. Lie-Wen Chen, Che Ming Ko, and Bao-An Li, Phys. Rev. C **72**, 064309 (2005).
26. S. Yoshida and H. Sagawa, Phys. Rev. C **73**, 044320 (2006).
27. C.-H. Lee, T. T. S. Kuo, G. Q. Li, and G. E. Brown, Phys. Rev. C **57**, 3488 (1998).
28. B. K. Agrawal, Phys. Rev. C **81**, 034323 (2010).
29. P. Sarriguren, M. K. Gaidarov, E. Moya de Guerra, and A. N. Antonov, Phys. Rev. C **76**, 044322 (2007).
30. M. K. Gaidarov, A. N. Antonov, P. Sarriguren, and E. Moya de Guerra, Phys. Rev. C **84**, 034316 (2011).
31. M. K. Gaidarov, A. N. Antonov, P. Sarriguren, and E. Moya de Guerra, Phys. Rev. C **85**, 064319 (2012).
32. D. Vautherin, Phys. Rev. C **7**, 296 (1973).
33. E. Moya de Guerra, P. Sarriguren, J. A. Caballero, M. Casas, and D. W. L. Sprung, Nucl. Phys. **A529**, 68 (1991).
34. E. Chabanat, P. Bonche, P. Haensel, J. Meyer, and R. Schaeffer, Nucl. Phys. **A635**, 231 (1998).
35. N. Van Giai and H. Sagawa, Phys. Lett. **B106**, 379 (1981).
36. M. Beiner, H. Flocard, N. Van Giai, and P. Quentin, Nucl. Phys. **A238**, 29 (1975).
37. L. G. Cao, U. Lombardo, C. W. Shen, and N. Van Giai, Phys. Rev. C **73**, 014313 (2006).
38. F. Le Blanc *et al.*, Eur. Phys. J. A **15**, 49 (2002).
39. F. Le Blanc *et al.*, Phys. Rev. C **72**, 034305 (2005).

40. M. Anselment, K. Bekk, A. Hanser, H. Hoeffgen, G. Meisel, S. Goring, H. Rebel, and G. Schatz, Phys. Rev. C **34**, 1052 (1986).
41. C. Piller, C. Gugler, R. Jacot-Guillarmod, L. A. Schaller, L. Schellenberg, H. Schneuwly, G. Fricke, T. Hennemann, and J. Herberz, Phys. Rev. C **42**, 182 (1990).
42. B. Nerlo-Pomorska and B. Mach, At. Data Nucl. Data Tables **60**, 287 (1995).
43. G. Fricke *et al.*, At. Data Nucl. Data Tables **60**, 177 (1995).
44. M. Keim, E. Arnold, W. Borchers, U. Georg, A. Klein, R. Neugart, L. Vermeeren, R. E. Silverans, and P. Lievens, Nucl. Phys. **A586**, 219 (1995).
45. K. A. Brueckner, J. R. Buchler, S. Jorna, and R. J. Lombard, Phys. Rev. **171**, 1188 (1968).
46. K. A. Brueckner, J. R. Buchler, R. C. Clark, and R. J. Lombard, Phys. Rev. **181**, 1543 (1969).
47. A. N. Antonov, V. A. Nikolaev, and I. Zh. Petkov, Bulg. J. Phys. **6**, 151 (1979); Z. Phys. A **297**, 257 (1980); *ibid* **304**, 239 (1982); Nuovo Cimento A **86**, 23 (1985); A. N. Antonov *et al.*, *ibid* **102**, 1701 (1989); A. N. Antonov, D. N. Kadrev, and P. E. Hodgson, Phys. Rev. C **50**, 164 (1994).
48. A. N. Antonov, P. E. Hodgson, and I. Zh. Petkov, *Nucleon Momentum and Density Distributions in Nuclei* (Clarendon Press, Oxford, 1988).
49. A. N. Antonov, P. E. Hodgson, and I. Zh. Petkov, *Nucleon Correlations in Nuclei* (Springer-Verlag, Berlin-Heidelberg-New York, 1993).
50. A. N. Antonov, D. N. Kadrev, M. K. Gaidarov, E. Moya de Guerra, P. Sarriguren, J. M. Udias, V. K. Lukyanov, E. V. Zemlyanaya, and G. Z. Krumova, Phys. Rev. C **72**, 044307 (2005).
51. http://hallaweb.jlab.org/parity/prex.
52. S. Abrahamyan *et al.*, Phys. Rev. Lett. **108**, 112502 (2012).
53. A. Tamii *et al.*, Phys. Rev. Lett. **107**, 062502 (2011).
54. O. Moreno, E. Moya de Guerra, P. Sarriguren, and J. M. Udias, J. Phys. G **37**, 064019 (2010).
55. C. J. Horowitz *et al.*, Phys. Rev. C **85**, 032501(R) (2012).
56. X. Roca-Maza, M. Centelles, X. Viñas, and M. Warda, Phys. Rev. Lett. **106**, 252501 (2011).
57. J. Piekarewicz, B. K. Agrawal, G. Colò, W. Nazarewicz, N. Paar, P.-G. Reinhard, X. Roca-Maza, and D. Vretenar, Phys. Rev. C **85**, 041302(R) (2012).
58. A. E. L. Dieperink, Y. Dewulf, D. Van Neck, M. Waroquier, and V. Rodin, Phys. Rev. C **68**, 064307 (2003).
59. A. E. L. Dieperink and P. Van Isacker, Eur. Phys. J . A **32**, 11 (2007).
60. Lie-Wen Chen, Phys. Rev. C **83**, 044308 (2011).
61. J. J. Griffin and J. A. Wheeler, Phys. Rev. **108**, 311 (1957).
62. M. B. Tsang *et al.*, Phys. Rev. C **86**, 015803 (2012).
63. M. Centelles, X. Roca-Maza, X. Viñas, and M. Warda, Phys. Rev. C **82**, 054314 (2010).
64. C. J. Horowitz, E. F. Brown, Y. Kim, W. G. Lynch, R. Michaels, A. Ono, J. Piekarewicz, M. B. Tsang, and H. H. Wolter, arXiv:1401.5839 [nucl-th].
65. A. N. Antonov *et al.*, Nucl. Instr. Meth. Phys. Res. **A637**, 60 (2011).